Construction Materials

GFRP durability appraisal: mechanical testing of naturally aged composite panels
Gates, Ibell, Darby and Evernden

ice | proceedings

Proceedings of the Institution of Civil Engineers

http://dx.doi.org/10.1680/jcoma.17.00023
Paper 1700023
Received 12/03/2017 Accepted 31/07/2017
Keywords: composite structures/service life/strength & testing of materials

ice Institution of Civil Engineers
publishing

GFRP durability appraisal: mechanical testing of naturally aged composite panels

1 **Pete Gates** BEng (Hons), PhD, CEng, MICE
Senior Structural Engineer, Smith Foster Limited, Poole, UK
(corresponding author: peter.gates@gatespremierstructures.co.uk)
(Orcid:0000-0002-5334-0936)

2 **Tim Ibell** FREng, CEng, BSc(Eng), PhD, FIStructE, FICE, FHEA
Professor, Department of Engineering, University of Cambridge, Cambridge, UK (Orcid:0000-0002-5266-4832)

3 **Antony Darby** BSc(Hons), PhD, CEng, MIStructE
Reader, Structural Engineering and Head of Civil Engineering Group, Department of Architecture and Civil Engineering, University of Bath, Bath, UK

4 **Mark Evernden** MEng, PhD, FHEA
Senior Lecturer, Department of Architecture and Civil Engineering, University of Bath, Bath, UK




The findings of a durability study undertaken on pultruded glass fibre reinforced polymer (GFRP) cladding panels are presented. Sourced at demolition from the Second Severn Crossing Visitors' Centre building in the UK, the panels offered the rare opportunity to assess the characteristics of naturally aged composite material. Mechanical properties were determined and compared with the properties of new, equivalent material. The phenomenon of polymer hardening, typified by a reduction in the material strain limit over time, was investigated by further mechanical testing procedures. By contrasting the properties as found for panels taken from each of the four external walls of the building, factors concerning environmental exposure and factors relating to the original fabrication conditions were investigated. The results indicate that, regardless of the exposure conditions, in 17 years the mechanical material properties appear not to have significantly diminished, despite aesthetic quality suffering due to lack of maintenance. It has, however, been shown that ultraviolet exposure causes a hardening of the resin component of the composite, resulting in an increase in the compressive elastic modulus, but a reduction in the threshold of the brittle fracture of the matrix in tension. This final result has not been documented before and is significant in understanding the long-term performance of composites.

Notation

A	cross-sectional area
A_s	shear area (effective cross-section area resisting shear)
a_s, b_s	locally applied point loads inducing shear in coupon specimen
B	web separation distance for thin-walled cellular panel section
b_w	web thickness for thin-walled cellular panel section
E_f	elastic Young's modulus of fibre reinforcement
E_{f_c}	compressive Young's modulus of fibre reinforcement
E_{f_t}	tensile Young's modulus of fibre reinforcement
E_m	elastic Young's modulus of polymer matrix
F	point load used to apply shear to a material coupon specimen
G_{xy}	shear modulus
I	second moment of area
l	span length
P	applied load, mid-span unless stated otherwise
r_y	radius of gyration
T	sectional depth
t_f	flange thickness
V_f	fibre volume ratio
w	deflection mid-span in z-axis direction
x	depth through section to neutral axis position
$\#_{\#c}$, $\#_{\#t}$	subscripts denote compressive and tensile nature of the property, as for elastic Young's modulus
$\#_r$, $\#_m$, $\#_f$	subscripts denote composite, polymer matrix and fibre reinforcement
α	inclination of strain gauge from principal fibre direction
γ_{xy}	shear strain in plane xy
ε	strain
τ_{xy}	shear stress in plane xy

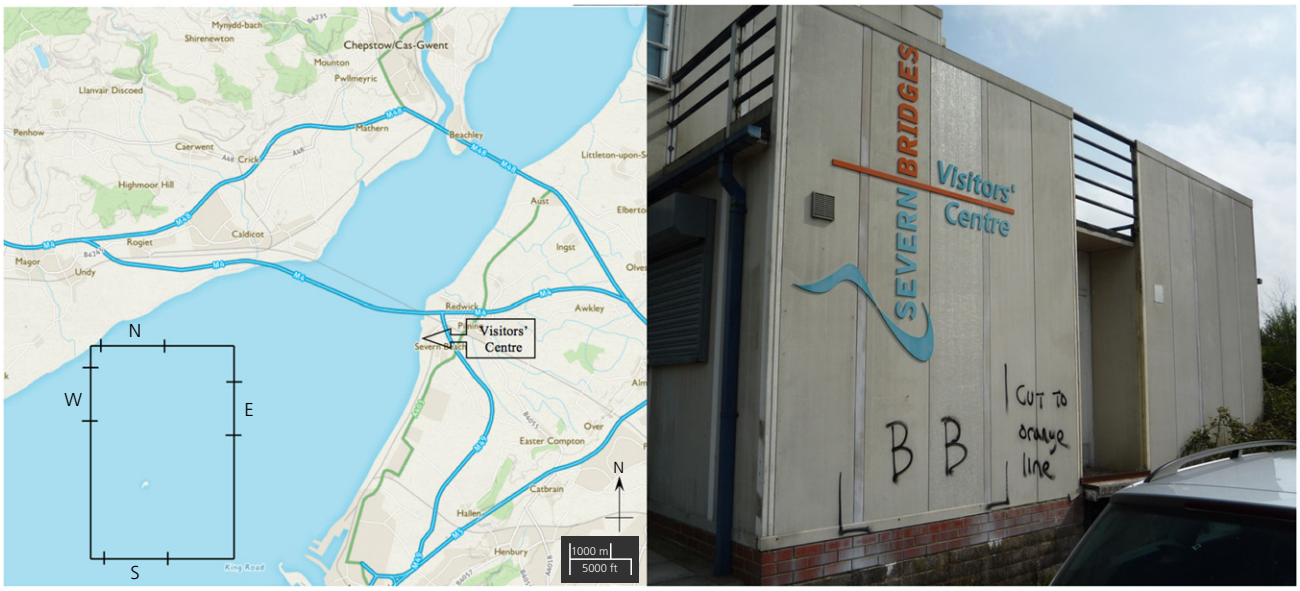

Figure 1. Location of the four 'panel pairs' from the Visitors' Centre at the Severn Crossing (OS, 2017) and photograph of the southerly elevation

1. Introduction

The long-term performance of fibre reinforced polymer (FRP) structures must be assessed if FRP is to win acceptance as a mainstream material for use in the construction industry (Busel, 2002). The environmental durability of wholly polymeric structures is often called into question. In response, accelerated testing is usually undertaken on artificially aged FRP specimens (Boinard *et al.*, 2000; Wang *et al.*, 2010); a lack of genuine naturally aged material has previously hindered the research and validation of material-related design life.

The eight panels tested in this investigation were produced by Maunsell Structural Plastics for application as enclosure panels for the deck of the second Severn Bridge. Leftover panels, described as 'factory seconds' by the manufacturer, were used to build a site office in 1993, which was later converted into the Visitors' Centre in June 1998, located in an exposed position near the Severn estuary (Figure 1). Two panels from each of the four principal facades were salvaged for testing, upon demolition in May 2009. N, E, S and W (north, east, south and west) denote the elevations from which the panels were taken. Tested in 2010, the results provide an account of pultruded glass fibre reinforced polymer (GFRP) panels naturally aged over 17 years.

This quantitative study assessing the mechanical material properties is intended to address the shortfall in the knowledge relating to naturally aged GFRP. The pultruded panels were

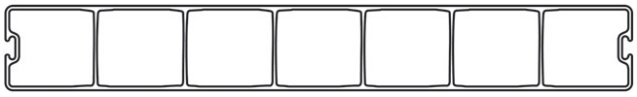

Figure 2. Strongwell panel cross-section (Strongwell, 2010)

tested whole, in flexure and cut to produce coupons of material for performing a range of mechanical tests. The results produced a profile of the material as a function of both its location within the section (internal flange web or external flange) and the exposure aspect of the original location on the Visitors' Centre building. Coupon testing using new, equivalent sample material provided a means to assess the mechanical property degradation attributed to exposure in a natural environment. Despite an exhaustive literature search, no 'base case' test data could be recovered to describe accurately the mechanical properties of the original panel material at the time of manufacture. It was therefore impossible to assess the environmental degradation in this way.

The prismatic cellular panels (now produced by Strongwell Ltd) are symmetrical in section (as shown in Figure 2) with an injected foam fill. The fill, which serves to provide a degree of thermal insulation, was applied to improve the environmental performance of the building and is not deemed to enhance structural function. The polymer matrix of the composite

Table 1. Panel geometric properties of both new and old panels from the manufacturer's design literature (Strongwell, 2010)

Second moment of area, I	6 620 000 mm^4
Area, A	5740 mm^2
Shear area, A_s	1790 mm^2
Section depth, T	80·3 mm
Radius of gyration, r_y	33·8 mm
Panel width	605 mm

material is polyester unsaturated isophthalic resin. The panel's geometric properties, as specified by the manufacturer for both the new and aged panels alike (these specifications have not changed), are shown in Table 1. It has been established, by conducting resin burn-off, that the fibre volume fraction, V_f, (e-glass fibres) of new panels is ∼0·36. Full details of fibre volume fractions for the flanges and webs of the new and old material are presented in Table 2. The volume fraction of fibres that act as principal longitudinal reinforcement is presented in Section 2.2.

Specific design information from the manufacturer concerning the details of the principal, secondary, chopped strand mat (CSM) and surface veil fibre volume fractions was not available. Such information is considered commercially confidential by pultrusion manufacturers.

Environmental factors that can cause degradation of the composite include ultraviolet (UV) irradiation, moisture absorption and thermal fatigue from both diurnal and annual cyclic variations (Compston and Dexter, 2008; Karbhari *et al.*, 2003). South-facing panels (Figure 1) will have experienced the greatest solar irradiation, while panels on the north-facing facade are expected to have endured the dampest conditions. Surface veils (a component present in new panels, responsible for creating a resin-rich surface layer during the pultrusion process to improve aesthetics and durability) were missing on the external face of the recovered panels, thus decreasing the expected long-term mechanical performance of this material. This concurs with the fact that these panels were earmarked as factory seconds and not used for the primary design purpose – that is, as a bridge enclosure. A comparative study using internal, external and web material from each of the facade elevations was carried out to establish the influence of environmental exposure on the mechanical performance of the GFRP pultrusions.

The value of the elastic modulus, E, when defined in the field of composites, can be $E_{tensile}$, $E_{compressive}$ or $E_{flexural}$ (Tolf and Clarin, 1984). This is essentially due to the difference between the tensile modulus and compressive modulus of the constituent materials. In this study, all forms of the elastic modulus of the aged material were determined by way of coupon tests. This allowed further exploration of the long-term properties of the constituent composite parts. Inspecting the results for these relative moduli was prompted further investigation into the occurrence of polymer hardening.

2. Methodology

The methodology used to investigate whole panels is presented first. This is followed by the methodology used for the calculation of the theoretical strengths and stiffnesses of the material at the coupon level, followed by coupon testing procedures. The results of the laboratory investigations are then presented in Section 3.

2.1 Whole panel testing

It was hypothesised that the differing degrees of environmental exposure (to UV irradiation for instance) on the four building facades would yield different reductions in mechanical properties. The properties pursued for comparison were the flexural elastic modulus E_{flex} and flexural shear modulus G_{flex}. By establishing the values of these properties for each of the

Table 2. Fibre volume fractions for the flanges and webs of new and old material

Coupon location	Total fibre volume fraction, V_f	Principal fibre volume fraction, V_{pf}	Standard deviation
Int flange E	0·40	0·24	0·014
Int flange S	0·38	0·26	0·024
Int flange W	0·40	0·24	0·046
Ext flange E	0·37	0·21	0·012
Ext flange S	0·40	0·26	0·015
Ext flange W	0·36	0·22	0·008
Ext flange N	0·38	0·24	0·003
Aged flange average		0·24	—
Web E	0·39	0·18	0·003
Web S	0·29	0·09	0·016
Web N	*0·38*	*0·16*	*0·087*
Aged web average		0·14	—
Flange new	0·36	0·25	0·041
Web new	0·34	0·24	0·026

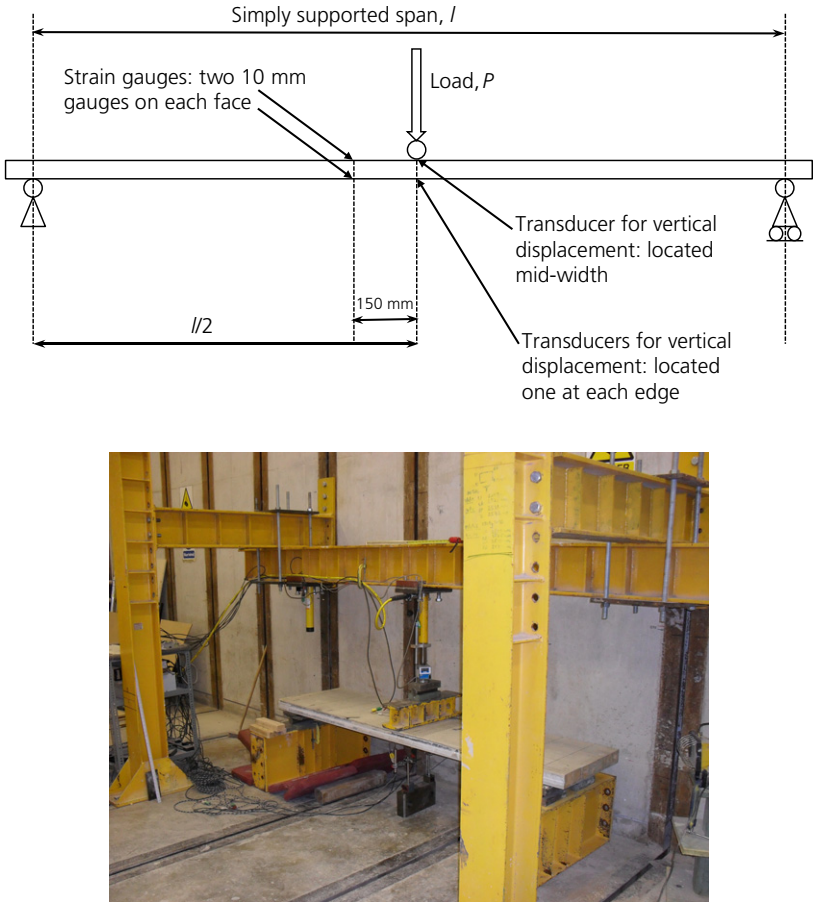

Figure 3. Three-point loading test rig set-up

panels, the extent of any mechanical deterioration attributed to exposure aspect can be assessed. Table 1 shows the sectional geometric properties of the tested panels.

A test rig for three-point bending was constructed, as shown in Figure 3. Strain gauges were attached to the panel faces at an offset of 150 mm from the central axis of the loading beam. Two gauges on each face (spaced at approximately quarter-width points, with one gauge over a web junction and one between two web locations) were applied to measure the average compressive and tensile strains across the width of the flanges. Three displacement transducers were set up across the panel width to measure the average mid-span deflection. Readings from all instrumentation were recorded every second during loading. Three bearing plates, all 150 mm wide, spanned the entire panel width, one under a pinned loading plate beneath the central loading actuator, and one at each end, consisting of a pin and roller support plate, forming the simply supported ends of the set-up, as shown in Figure 3.

To determine the flexural elastic modulus and shear modulus, E_{flex} and G_{flex}, a graphical method based on the Timoshenko beam theory for thin-walled sections (Bank, 1989) was adopted. Each panel was tested over three different spans consecutively before being turned over to repeat the testing. Timoshenko's beam equation can be rearranged to produce the relationship

$$1. \quad \frac{4Aw}{Pl} = \frac{1}{12E_{flex}}\left(\frac{l}{r_y}\right)^2 + \frac{1}{G_{flex}}$$

where l is the span length, P is the load applied, w is the mid-span deflection and the other variables are as per Table 1. Each load deflection result can be plotted on a graph of the type shown in Figure 4.

A three-point bending set-up was used so that a significant proportion of the resulting displacement was attributable to shear deflection and, as a consequence, the accuracy of the value obtained for shear modulus was improved.

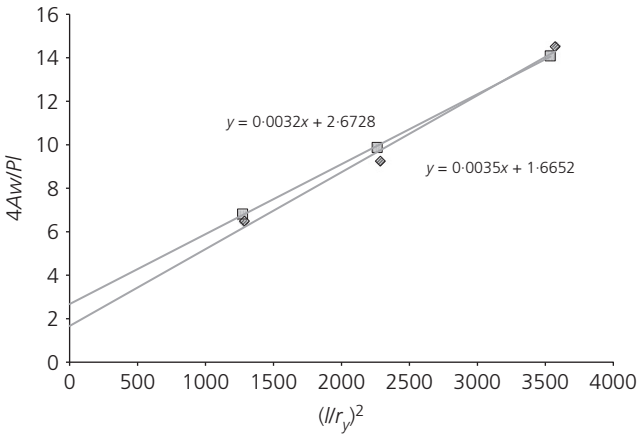

Figure 4. Graphical plot of Equation 1 for an east-facing panel (square symbols represent tests with external face up and diamonds represent tests with internal face up)

The flexural elastic modulus and flexural shear modulus can be inferred graphically from the gradient and vertical axis intercept, respectively.

The panel length dictated the maximum span for three-point testing to be 2·1 m with subsequent span reductions of 80% and 60%. Testing over these spans permitted the formation of plots such as that shown in Figure 4, producing three well-spread data points that were used to define the position of a line of best fit. The gradient of this line is equal in value to $1/12E_{\text{flex}}$ and the y-axis intercept is equal in value to $1/G_{\text{flex}}$. Hence, the values of the flexural elastic modulus and flexural shear modulus can be obtained.

Following the flexural tests detailed above, the panels were loaded to failure, using the longest of the three simply supported spans described previously. Panel pairs from each facade orientation were tested in alternate orientations in the test rig (one with the weathered external face uppermost and one with this face down-facing in tension, to observe the anticipated lower failure load when this face was in tension).

2.2 Determining relative theoretical mechanical properties by resin burn-off

The stiffness and strength of pultruded GFRP are closely related to fibre content. By establishing the fibre content of material from different parts of the panel cross-section and finding out if there is any inter-panel variation in the material fibre content, the relative performance of the coupons could be predicted in mechanical tests. Specimens for testing were cut from the webs and flanges of each of the panels. The specimens were 25 mm square in size, sourced at locations away from the flange–web junctions of the cellular panels.

(a)

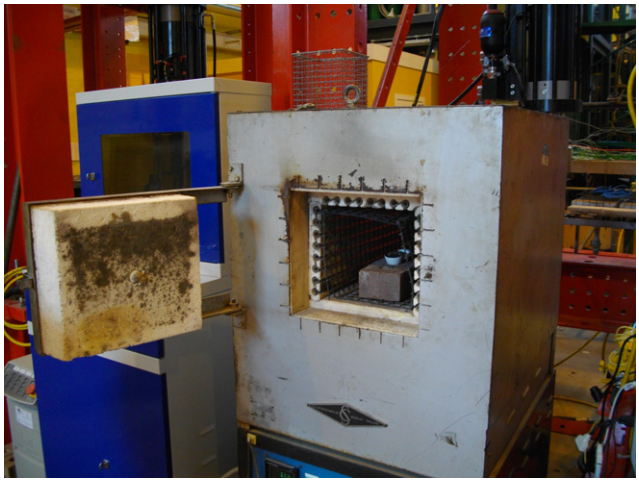

(b)

Figure 5. Sample ignited using a Bunsen burner (a), and then placed in a muffle furnace (b)

For both the aged and new material, resin burn-off to establish the fibre weight fraction was conducted according to ASTM D 2584-02 (ASTM, 2002). After weighing to find the initial mass of each of the 25 mm square samples, each sample was ignited by heating in a crucible over a Bunsen flame and left until the volatiles had cleared (once the smoke had stopped) and only fibres, ash and carbon remained. Each sample, in its own crucible, was then placed in a muffle furnace at 565°C for 6 h until all the carbonaceous material had disappeared (Figure 5). Re-weighing of the remaining

fibres yielded the fibre weight fraction; using values for the fibre and matrix density (2570 and 1200 kg/m^3, respectively (Bank, 2006)), the volume fractions could then be determined.

Principal fibres, CSM and surface veils (present only in the new composite panel material) were separated to enable more accurate calculation of volume fractions and subsequent theoretical mechanical properties, as recommended elsewhere (Ye *et al.*, 1995). Fillers were not removed, however, as this entails procedures of chemical washing and drying, such that the CSM fibre fractions are known to be overestimates.

Three samples were subjected to resin burn-off for each of the locations specified in the first column of Table 2. 'Int' denotes internal flange material (material from the interior facing surface of the panel), while 'Ext' refers to flange material that was taken from the exterior face of the panel.

Not all facade aspects are represented in this testing, but the aged panels were all manufactured to the same specification. While a degree of variation was observed between material from facades of different aspect and panel location (internal or external), it was the average fibre content values for flange and web material, of the new and aged panels, that were required to establish the desired theoretical properties of relative mechanical performance.

The volume fractions presented in Table 2 are the mean values derived from the results of three coupon specimens. The distribution of the principal fibres in many of the web elements tested was not uniform but, as illustrated in Figure 6, the principal fibres (seen as darker fibres in the image) in the web lay in bunches. Samples for testing taken from these webs captured various amounts of these fibres, rendering reduced confidence in the average value yielded. This was especially true for web samples taken from panels originally on the north-facing facade. The results from the coupons taken from the north-facing facade web elements (shown in italic in Table 2) were therefore not included in the averages for aged webs.

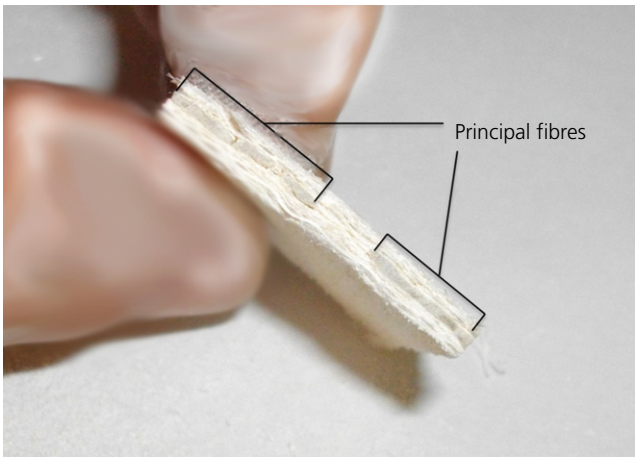

Figure 6. Principal fibres visible within the aged web coupon cross-section, after removal from furnace. Principal fibres are in the direction perpendicular to the page

New composite panels appear to be fabricated with a similar proportion of principal fibres in the flange and the web elements (bottom two rows of Table 2). The aged panels, although possessing a similar fibre content in the flanges, exhibited reduced fibre fraction in the webs. Thus, the stiffness and strength predicted for the aged webs were ~67% those of the aged flanges, which is indicative of how they were manufactured. It should be noted that a reduced amount of principal fibres was found to exist in the web elements from the southern facade panel tested and, as with other webs examined, the distribution was not uniform. This indicates a high degree of inter-panel variation in the manufacturing of the webs in the aged panels, as well as intra-panel variation.

The resin burn-off results suggest that the variation in mechanical performance observed between the new and aged flanges is a consequence of ageing rather than differing fibre content. One large manufacturing difference is evident. In Figure 7, the additional layer (surface veil) present in the new material can be distinguished easily by eye, from the CSM and the principal fibres, once removed from the furnace.

2.3 Tensile testing of coupons

To compare the mechanical properties of material from different panel location and to compare new and old material, the axial tensile strength and modulus were determined by fabricating and testing coupons in tension. These properties are influenced mainly by the fibre component.

Three coupons representing each of the internal and external flange material, and web material, for each facade aspect, were cut from near the panel ends, which had not experienced significant bending stresses from the previous whole panel testing (<20 MPa; ~10% of the ultimate tensile strength defined by Strongwell (2010)). The average thickness of the flange coupons was 3·15 mm and that of the web coupons was 2·66 mm. The precise cross-sectional geometry of each coupon was measured using Vernier calipers. Coupons were sized 25 mm wide × 250 mm long according to BS EN ISO 527 (BSI, 2009), with the pultruded fibres (0° fibres) aligned along the coupon length. Aluminium tabs of 1·5 mm thickness and 50 mm length were bonded to the coupon ends (in the area in contact with the test rig jaws) using epoxy resin. A single 10 mm strain gauge was attached centrally on each face of the

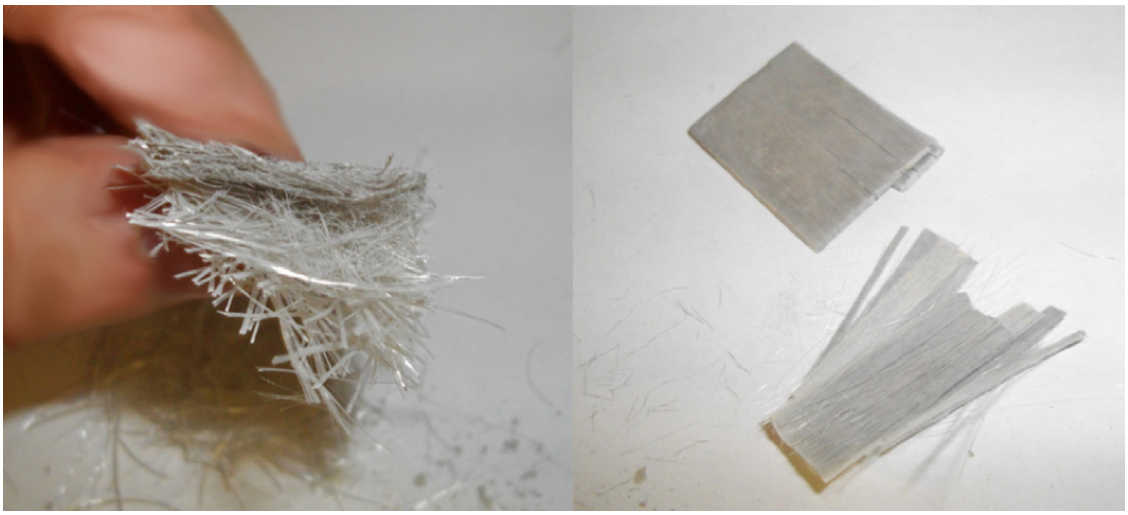

(a) (b)

Figure 7. Fibres from new material: (a) surface veil over CSM; (b) principal fibres

coupon, orientated in the direction of the applied load. Testing was conducted under displacement control at 1 mm/min, in line with both manufacturer testing and the code-based approach adopted. Coupons extracted from new, equivalent panels, manufactured by Strongwell, were also tested for comparison.

2.4 Compressive testing of coupons

To compare further the mechanical properties of the various categories of material (as described above), the axial compressive modulus was determined. This property is influenced more by the resin component than tensile properties are, and so permits the opportunity to assess the environmental degradation of the resin.

A test rig used to clamp the ends of the coupons was fabricated to prevent rotation while loading the sample through its ends, as shown in Figure 8. For testing in compression, the overall coupon length was 165 mm (again, aligned such that the pultruded fibres were aligned along the coupon length) and the width was 10 mm, with 70 mm of each end clamped in the rig and 25 mm left clear. Strain gauges were attached, one to each face of the coupon, in this free region. Testing was again conducted under 1 mm/min displacement control. The results for ultimate compressive stress are not included here, only the compressive elastic modulus, because buckling prevented determination of accurate material compressive strength. Shorter specimens would have enabled ultimate compressive stress to be established, however they would require smaller gauges that would not be accurate in determining the elastic modulus. Further tests would be required to achieve this.

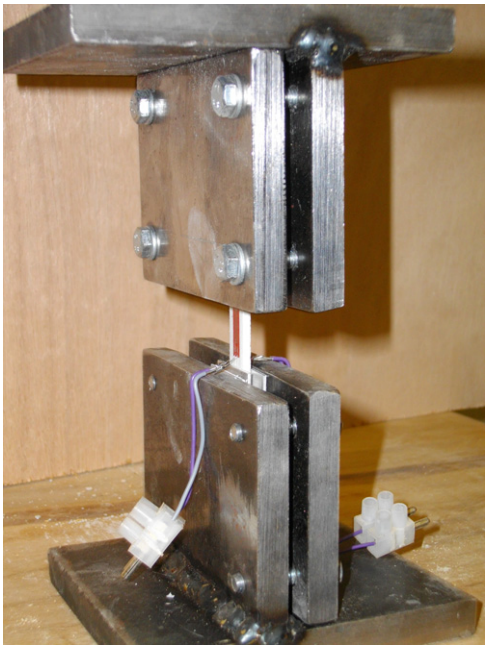

Figure 8. Coupon set-up for compression test rig

2.5 Shear testing of coupons

Shear testing is a resin-dominated mechanical test of the composite material. The Iosipescu shear test (VPG, 2008) procedure was adopted to perform testing. A custom rig was designed to accommodate suitable coupon sizes and to apply a shear force in line with the Iosipescu methodology, as

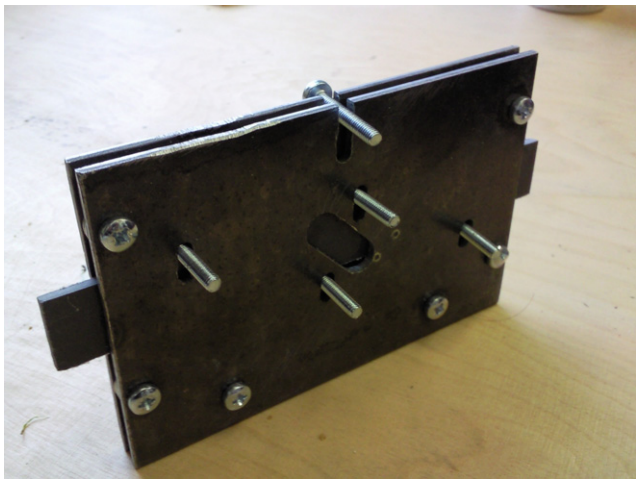

(a)

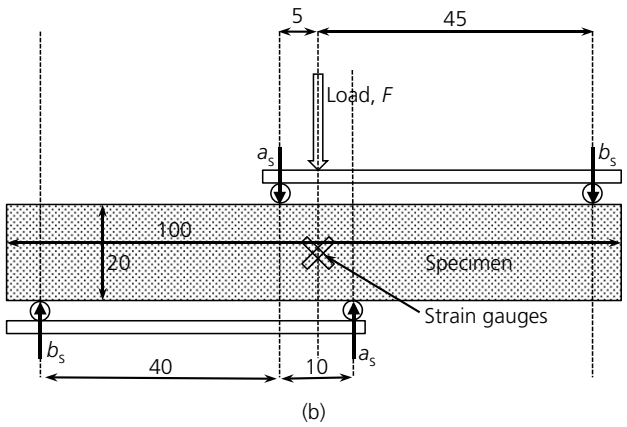

(b)

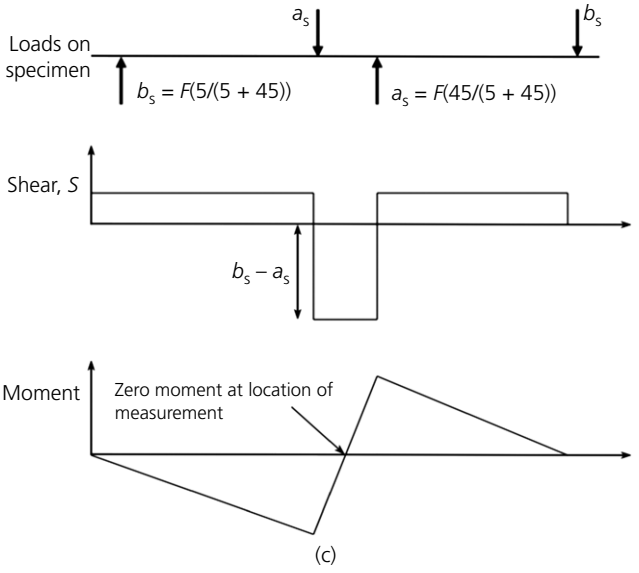

(c)

Figure 9. (a) and (b) Iosipescu shear rig set-up (all dimensions in mm). (c) Schematic diagram showing how loads on specimen are achieved and shear is derived at zero moment location

shown in Figure 9. Principal (0°) fibres were once again aligned parallel with the longitudinal specimen direction (perpendicular to the load direction). Two steel plates provided out-of-plane stability to the test specimen. The specimens were 20 mm wide × 100 mm long. Top and bottom steel loading bars, together with a pin arrangement, enabled loading to be applied to produce the maximum shear and zero moment at the centre point of the test coupon. An observation window cut-out allowed strain gauges to be located. The pins were located within long slotted holes to guide them, avoiding the need to notch the sample at the pin locations, which could otherwise have caused unwanted stress concentrations due to the notch inhibiting lateral movement of the pin across the surface under flexure. The specimen was loaded by means of a mass hanger and weights, with the load applied through the top pin of the rig. Loading was limited to 80 kg by the strength of the loading system, and it was found that this could be applied accurately without damaging the rig. The geometry of the loading arrangement resulted in a shear force in the measured region of 80% of the applied load, as shown by Equation 2 and illustrated in Figure 9

$$\text{2.}\quad \text{Shear} = b_s - a_s = 0{\cdot}9F - 0{\cdot}1F = 0{\cdot}8F$$

where a_s and b_s are locally applied point loads inducing shear in the specimen.

Readings from two perpendicular 45° strain gauges were recorded and the shear modulus G_{xy} was calculated according to

$$\text{3.}\quad G_{xy} = \tau_{xy}/(\varepsilon_1 - \varepsilon_2)$$

where ε_1 and ε_2 are strains from the two perpendicular gauges inclined at 45° to the horizontal and τ_{xy} is the shear stress at mid-depth of the section found from the section dimensions, and the shear force as per Figure 9. Equation 3 is true for any inclination of the shear plane in the specimen (as a result of variation in the specimen depth), provided that the gauges are centred at mid-depth at the point of contraflexure of the specimen.

Equation 4, taken from a technical note for use of strain rosettes in performing Iosipescu tests (VPG, 2008), accounts for the influence of the vertical compressive strain when using gauges inclined at 45° to determine shear strain, γ_{xy}, where α is the inclination angle of the gauge, thus explaining why γ_{xy} is represented as (ε_1–ε_2) in Equation 3

$$\text{4.}\quad \gamma_{xy} = (\varepsilon_1 - \varepsilon_2)/\sin 2\alpha$$

3. Results

3.1 Design values for new Composolite panel properties

The design values for the panels, as manufactured today with product name 'Composolite', as stated in the Strongwell design literature (Strongwell, 2009). Table 3 shows the values related to stiffness and strength. Also obtained from the manufacturer's literature are the results of three-point bending tests performed on complete panels, equivalent to the testing undertaken on the aged panels. By performing the graphical method describing Timoshenko beam theory on these results, further values (also included in Table 3) were established for comparison.

3.2 Whole panel testing: flexural elastic modulus

Figures 10 and 11 provide a summary of results concerned with flexural stiffness. Each bar represents the value for a single panel.

Figure 10 shows that the panels that experienced direct UV irradiation (on the east-, south- and west-facing building elevations) exhibited a lower stiffness when tested in bending with the exposed external face in tension. The north-facing panels did not show this behaviour. This suggests that degradation attributed to UV exposure or cyclic wetting and drying is of greater detriment to material stiffness when compared with damp conditions alone. It also suggests that in tension the matrix is compromised, however, in compression it is not.

Examining the results in Figure 11, the calculated flexural shear modulus appears to be sensitive to the nature of testing of the panel (inverted or not). However, it has previously been documented (Tolf and Clarin, 1984) that the shear modulus values derived using the graphical method employed are sensitive to small changes in the fit of the regression line. Considered mathematically, the adopted Timoshenko equation for beam bending produces a solution for flexural shear modulus that is highly sensitive to small changes in the input variables, due to the small contribution of shear deformation to the total deflection. The average shear modulus measured appears to meet that of the manufacturer's value for modern panels (Figure 11).

Table 3. GFRP material properties (Strongwell, 2009)

Strongwell design literature (minimum values)	
Tensile elastic modulus, E	17·1 GPa
Ultimate tensile strength	214 MPa
E_{flex} and G_{flex} inferred by the graphical method from Strongwell's in-house load–deflection test results	
Flexural elastic modulus, E_{flex}	25·3 GPa
Flexural shear modulus, G_{flex}	0·95 GPa

3.3 Coupon testing: tensile modulus

Figure 12 shows the results for coupons taken from the panels and tested in tension. The web material of the aged panels appears to have a lower tensile modulus than the flanges, although this difference was not evident in the new material. This is as predicted by resin burn-off and hand calculations. The lowest value of tensile elastic modulus established during testing was 15 GPa (for the south-facing panel web coupons). This correlates well to the established reduction in the fibre content of these elements, as illustrated in Table 2. The coupons of the internal material outperformed those of the external material from both the south- and west-facing panels

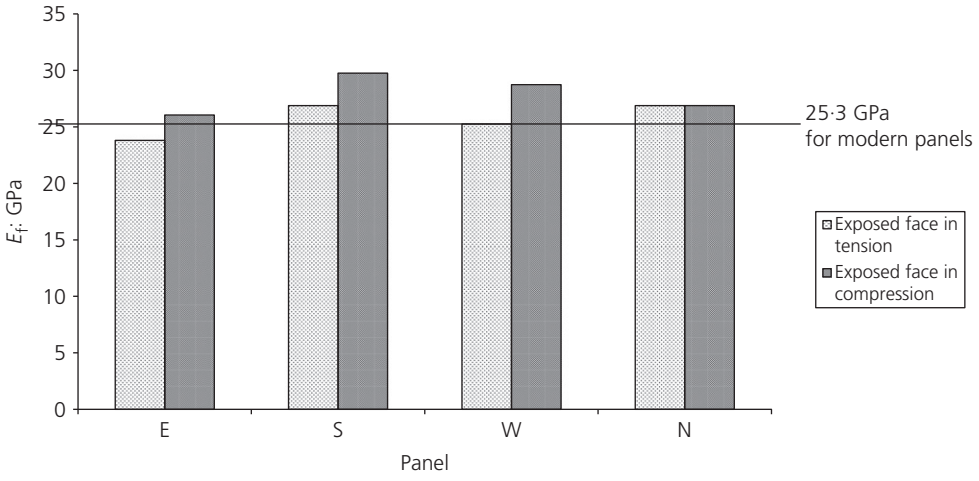

Figure 10. Flexural elastic modulus for each of the building panels and the manufacturer's testing-derived value of 25·3 GPa

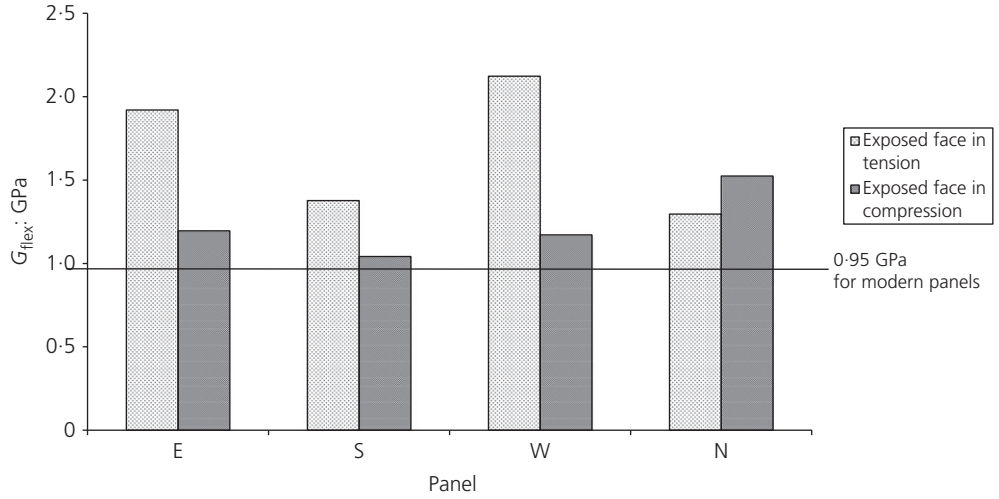

Figure 11. Flexural shear modulus G_{flex} for each panel, as per original orientation on building and nature of test, and the manufacturer's testing-derived value of 0·95 GPa

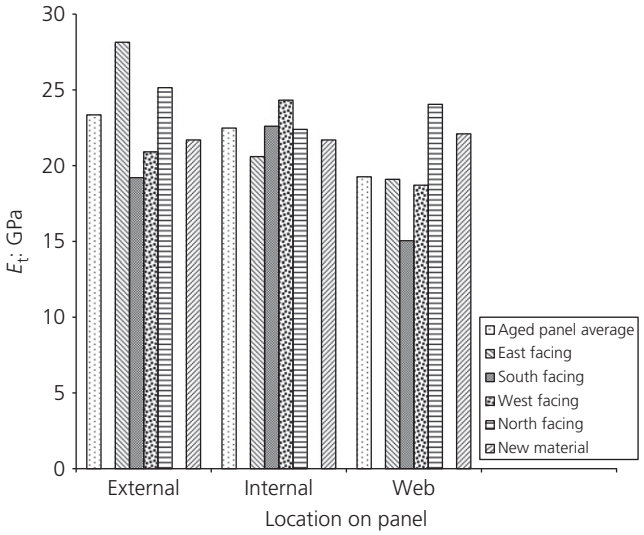

Figure 12. Tensile elastic modulus as a function of coupon origin

subjected to the prevailing estuary wind. Coupons from the north- and east-facing panels did not exhibit this trend. A large variance across the tests was observed, particularly for the webs (as already discussed) and external material, prompting further investigation. In Figure 12, each result represents the average from three coupon tests.

Figure 13 shows a high degree of linearity to failure in the stress–strain response of the pultruded GFRP to axial tensile load. It should be noted that not all of the plots presented in this figure represent the material load to failure due to strain gauges going off-scale or breaking from the specimen. The tensile elastic modulus was calculated using a strain of 2000 με.

3.4 Coupon testing: tensile strength

Figure 14 shows the strength of the material from different panel origins (each result represents an average from three coupon tests). Coupons of the external flange material generally exhibited a lower strength than the internal material, indicative of environmental degradation. Material that was exposed on the south-facing building facade showed the biggest reduction in strength. This material had been subjected to the most UV irradiation.

As also found in the tests measuring tensile elastic modulus, webs from the south-facing panels tested gave a low result, by chance equal to the lower-bound manufacturer's design value (214 MPa), which again, correlates well with the reduced fibre content seen in these elements from the resin burn-off tests.

Tensile strength and modulus exhibited similar trends, indicating that perhaps fibre volume is responsible for the variation, rather than degradation. However, Table 2 shows that this is probably not the case and that environmental degradation is indeed responsible. The south-facing external flange material that was subjected to resin burn-off possessed the highest fibre content. The crucial finding here is that the average aged-panel tensile capacity (293 MPa) was significantly lower than the new-panel tensile capacity (321 MPa).

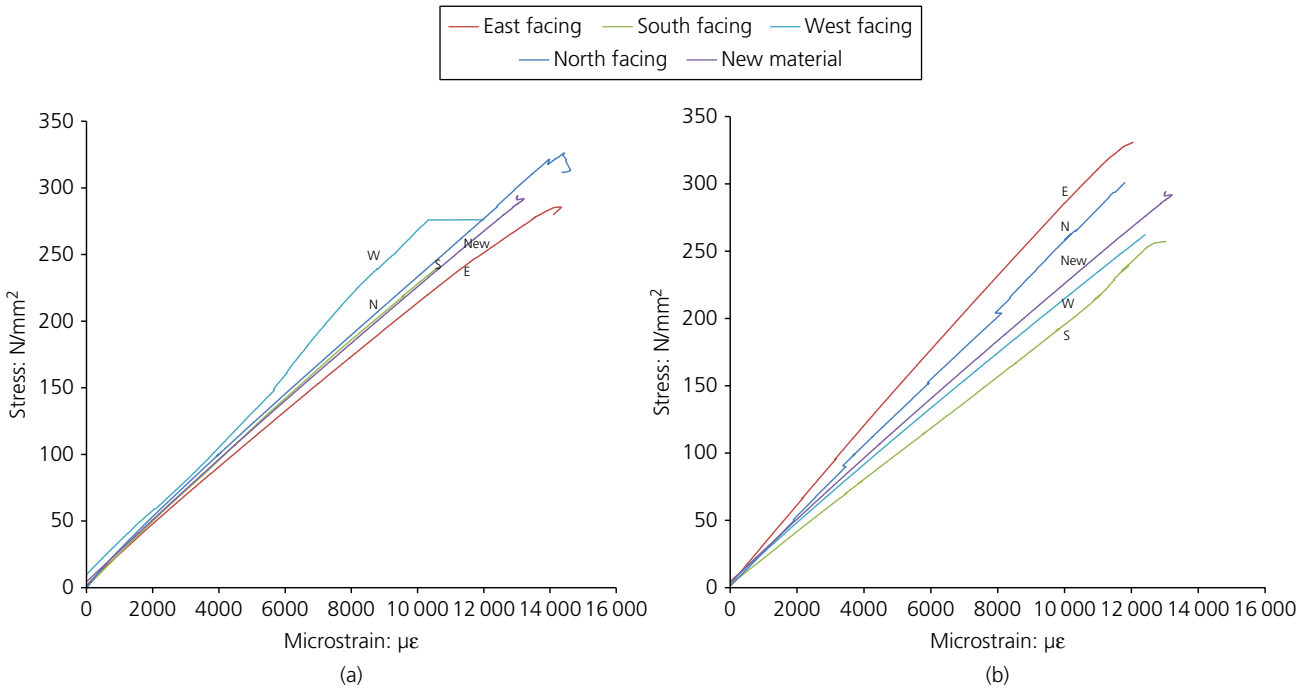

Figure 13. Stress–strain plots, for internal (a) and external (b) panel material

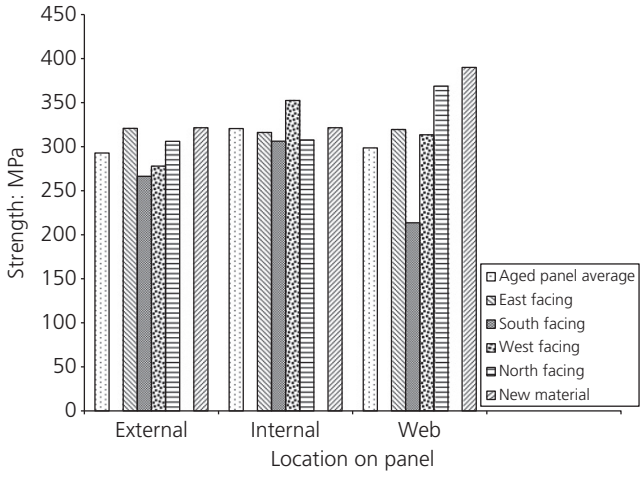

Figure 14. Maximum tensile strength of coupons

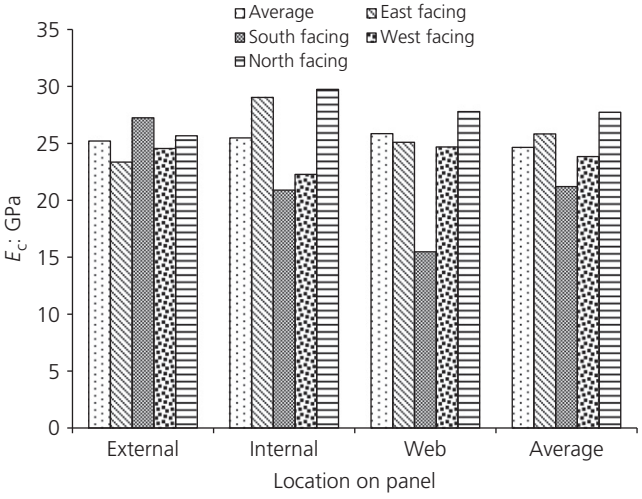

Figure 15. Compressive modulus, E_c, as a function of coupon origin

3.5 Coupon testing: compressive modulus

The compressive modulus data presented in Figure 15 are the minimum values determined from two coupons tested to establish each data point. A high level of variation was observed for the two coupons tested for south-facing panel webs (41·9 and 15·5 GPa, resulting in a standard deviation of 18·7 GPa). This supports the existence of a non-uniform distribution of principal fibres in the web material of the south-facing panels (the next largest standard deviation of only 3·7 GPa was for web coupons from the east-facing panels). The fabrication variability in this web material, attributed to their reduced quality (they were 'factory seconds') is seen to impinge on the mechanical properties. The limited width of the coupons extracted (10 mm for compressive testing) and

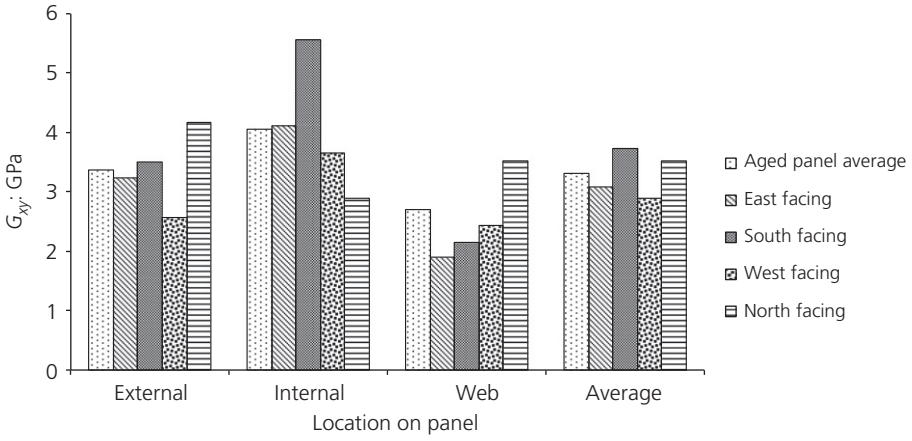

Figure 16. Shear modulus as a function of coupon origin

the distribution of the fibres in the webs, as shown in Figure 6, are understood to permit large variations in the amount of fibre 'captured' in the prepared test specimen. Thus, the degree of variability exhibited in the results for web specimens is amplified.

The overall average compressive elastic modulus of 26·8 GPa was 17·5% higher than the tensile modulus given in Section 3.3. It is more usual that the compressive modulus is lower than the tensile modulus for FRP materials (Bank, 2006), so this suggests that, in this case, resin plays an important part in the behaviour. The resin component could be contributing to compressive stiffness to a greater extent than to tensile stiffness, due to physical change with age. This hypothesis is explored further in Section 4.

No new material was available at the stage of compression testing for comparison. A standard deviation of 2·1 GPa was found for the average results relating to the panels on the different facades, in both tensile and compressive testing for elastic modulus. In tension, however, the panel webs displayed a lower average stiffness compared with the panel flanges, which was not evident in the results for compressive testing. This suggests that the resin has a greater influence on the compressive modulus measured than on the tensile modulus.

3.6 Coupon testing: shear modulus

Figure 16 shows the results of the shear modulus coupon tests. It can be seen that the west-facing panels exhibited the lowest average shear modulus. The lack of stiffness of the webs in this panel is not likely to be attributed to deterioration with age, as the exterior material maintained good integrity. Internal coupons were observed to be stiffer than external coupons by 17%, although the averages displayed were significantly affected by the high result for the internal coupons from the south-facing panels.

3.7 Flexural strength of whole panels

A theoretical model was derived, from first principles, for the bending stiffness of the cellular panels (of the type detailed in Section 3.2) (Figure 17). Previous studies have reported that the axial compressive stiffness is typically 80% of the tensile stiffness (Bank, 2006), and the model takes into account this ratio of the differing compressive and tensile axial elastic modulus of the fibres in GFRP. It has been demonstrated in Section 3.2 that aged resin influences the relative compressive and tensile elastic moduli to an extent where the fibre behaviour does not yield a similar effect on composite stiffness. This section describes work undertaken with the intention of comparing the failure stresses of each of the panels, and also comparing the theoretical flexural response of the panels according to a compressive/tensile modulus ratio from the literature with the measured experimental response. However, the second objective was not possible, for reasons explained later. It has been shown that the model developed to describe the stress and strain in a composite section is useful in comparing the performance of panels from each facade orientation in order to determine whether environmental exposure influenced the ultimate collapse load.

$$
\begin{aligned}
&x^2\left[E_{f_c}\left(\frac{b_w}{2B}\right)V_f + E_m\left(\frac{b_w}{2B}\right)(1-V_f)\right] \\
&-(T-x)^2\left[E_{f_t}\left(\frac{b_w}{2B}\right)V_f + E_m\left(\frac{b_w}{2B}\right)(1-V_f)\right] \\
&+(T-x)[E_{f_t}t_fV_f + E_mt_f(1-V_f)] \\
&-x[E_{f_c}t_fV_f + E_mt_f(1-V_f)] = 0
\end{aligned} \qquad (5)
$$

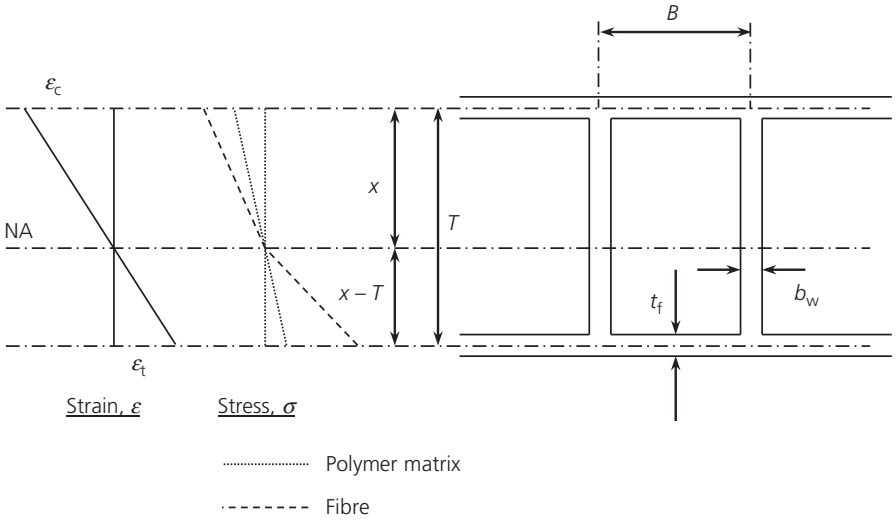

Figure 17. Stress block for FRP thin-walled section

Table 4. Composolite panel properties necessary to determine the neutral axis depth and resistive moment per unit surface strain, as calculated theoretically

T: mm	B: mm	t_f: mm	b_w: mm	V_f	E_m: GPa	E_{f_t}: GPa	E_{f_c}/E_{f_t}	E_{f_c}: GPa	x: mm	M/ε/unit width: kNmm/mm
77·1	85	3·15	2·66	0·67	3·6	75	0·8	60	44·0	9800

Table 5. Failure strain and stress, derived from load, test span and theoretical distribution of stress

Panel facade	Nature/orientation	Failure load: kN	Length of span: mm	Moment per unit width: kNmm/mm	Compressive strain (as per Table 4): με	Compressive fibre stress (as per E_{f_c} = 60 GPa): MPa
E	Int in compression	36·8	2010	30 571	3120	187
	Ext in compression	52·1	2010	43 282	4417	265
S	Int in compression	49·5	2090	42 815	4369	262
	Ext in compression	40·5	2100	35 200	3592	216
W	Int in compression	34·5	2090	29 810	3042	183
	Ext in compression	43·0	2110	37 499	3826	230
N	Int in compression	37·1	2560	39 259	4006	240
	Ext in compression	32·4	2550	34 182	3488	209
Average		—	—	—	—	224

Table 4 shows the values of the panel properties that were necessary to determine the neutral axis depth and the moment of resistance per unit surface strain according to Equation 5 (from which the neutral axis x may be found) and the stress distribution in Figure 17. The resulting value of 9800 kNmm/mm was used together with the three-point test span and the predicted failure load found experimentally for each panel to provide an expected strain at failure on the compressive upper panel face. Note that the value 9800 kNmm/mm is moment per unit width per unit strain on the surface in compression. Table 5 shows how this was used to determine failure strains and stresses: the values of compressive strain were found from the moment per unit width of panel divided by 9800 kNmm/mm.

The model shown in Figure 17 allows comparison of theoretical values of surface strains with the values measured in the laboratory. Table 6 shows this expected strain at failure, alongside the average measured strain at failure from the two gauges on the upper surface of each panel.

Table 6. Compressive strain at failure for each panel and orientation, based on failure load and theoretical model, alongside the average of two strain gauge measurements

	Strain at failure: με			
	Internal face up		External face up	
Panel	Predicted from model	Measured	Predicted from model	Measured
E	3120	2510[a]	4420	4010[a]
S	4370	3840[a]	3590	3120[a]
W	3040	2870	3830	3540[a]
N	4010	—	3490	3100

[a]Gauge peeled from the specimen or went off-scale prior to failure, so that the value represents the single remaining gauge measurement

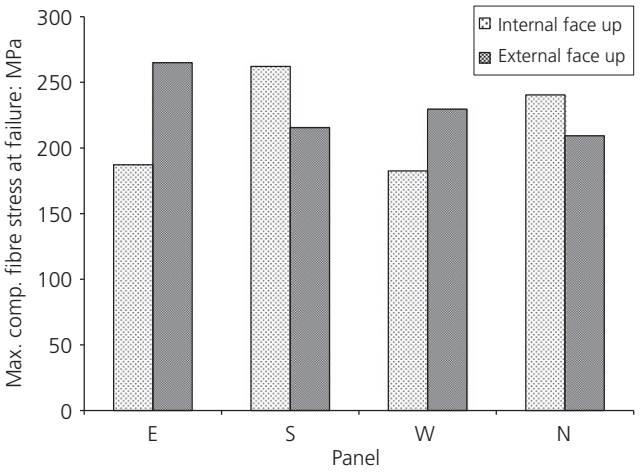

Figure 18. Maximum compressive fibre stress at failure of the whole panel in three-point bending

It can be seen from Table 6 that the measured strains were below those predicted by the theoretical model. This implies that the neutral axis position was closer to the compressive face than expected at (or just before) failure.

To quantitatively assess the extent to which the neutral axis had migrated from its expected position, more accurate strain gauge readings would be required. It is concluded that the work above cannot verify this. However, the findings do seem to align with previous results in this paper indicating that the GFRP polymer matrix was susceptible to brittle fracture in tension (causing the neutral axis to be closer to the compressive face than expected).

The results obtained for failure strain using the theoretical model are of much greater use to compare stress in the panels at failure; relying not on strain gauges, but on measured load, and panel and testing geometries. Figure 18 shows the data inferred by the failure load and the model.

The strength of the panels does not appear to be affected by the original aspect or orientation of testing, as seen with the stiffness of the whole panels. However, it should be noted that failure of the panels occurred by flange buckling with accompanying tearing of the flange web junction. This type of failure is very unstable and sensitive to a large number of variables. The large scatter in results attributed to this means that a larger number of panels would need to be tested to destruction to make the same kind of conclusions regarding the influence of environmental exposure as could be made regarding the stiffness of the whole panels.

4. Assessment of polymer hardening

4.1 Introduction

Brittle hardening of the polymer resin appears, from the results in this paper, to have significance in relation to the whole-life performance of GFRP. This is not a phenomenon that has been documented as being significant in the existing literature.

Upon inspection of the results from coupon testing, the measured compressive elastic modulus (26·6 GPa mean value) was found to be higher than the tensile modulus found for the material (22·1 GPa mean value). An entirely opposite relationship had been expected, since micro-buckling of fibres typically reduces the elastic modulus in compression; a value in compression of ∼80% that of the tensile modulus is more typical (Bank, 2006). It was hypothesised that brittle hardening of the resin over time may be responsible. The external material from the south-facing panels, which had experienced a higher degree of UV irradiation, exhibited the highest modulus. Hardening of the resin with age, and with UV exposure, could explain a higher modulus when working in compression. Such hardening could result in a reduced stiffness in tension due to early onset of brittle facture in the resin, whereas in compression no such fracture occurs. To investigate this hypothesis, further experimental work was undertaken.

4.2 Procedure for assessment of polymer hardening

Three coupons of aged GFRP external flange material, from south-facing panels, and five coupons of new GFRP panel flange material were subjected to two identical flexural tests (Figure 19), each with intervening tensile loading. Tensile loading was undertaken in accordance with the method described previously in Section 2.3, but with samples 330 mm in overall length. The tensile strain to which each coupon was subjected was varied according to the values indicated in Tables 7 and 8. The influence of the direct axial tensile strain

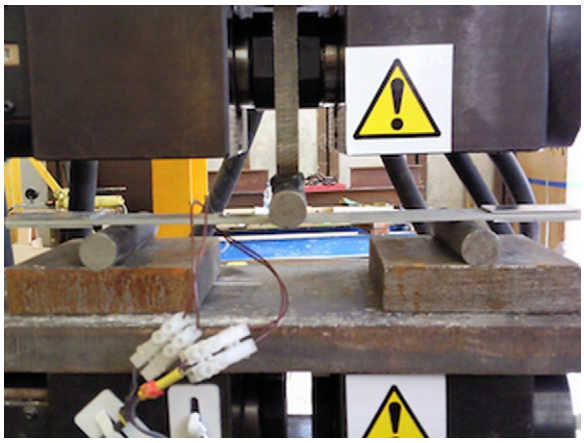

Figure 19. Flexural testing of coupon

could be observed by changes in the response of the subsequent flexural tests – that is, if resin plasticity was preserved there should be no fracture of the resin and the initial and final flexural tests would have identical flexural moduli. If UV degradation of the resin over the material lifetime had caused brittle hardening, and the strain limit of tensile fracture of the resin was exceeded, then a difference between the two flexural responses (pre- and post-tensile test) would be evident.

These flexural tests were conducted over a 200 mm span such that the strain in all material remained below 4000 με, which corresponds to a stress of 87 MPa (41% of the 214 MPa design ultimate strength). Using the second moment of area of the coupon cross-section and the applied load, the stress at the strain gauge location was derived. The corresponding strain recorded on the surface of the coupon at this same position (20 mm from the centre of the specimen) was then used to establish the flexural elastic modulus of the sample.

4.3 Results

The initial stiffness values of the three coupons of the aged-panel material, shown in Table 7, were found to be similar. The subsequent stiffnesses varied, depending on the axial tensile strain to which the specimens were subjected before being retested in flexure.

It can be seen that a tensile strain of 6000 με had no detrimental effect on the residual flexural stiffness of the sample; however, by imposing a strain of 9000 με the subsequent stiffness was almost halved. Sample 3 was strained to 10 000 με and the subsequent stiffness was shown to be very low. A reduction in stiffness this large would appear at first glance to be attributable to more than resin fracture, as the resin area in cross-section was only 30% of the total area. Indeed, in the case of sample 3 some fibre breakage could be heard. This did not occur during the straining of sample 2. Attributing such reductions in stiffness to the resin alone could be explained, and accounted for, by considering the fibre distribution in the coupon. It was established that the fibre distribution in the cross-section of pultruded GFRP elements was not uniform; the outer ply regions were more resin rich and the central lamina more fibrous. It could therefore be understood how flexural tests might be more sensitive to resin integrity, as the resin is more abundant in the regions that were more highly strained during flexure.

Further tests on new composite material, presented in Table 8, were necessary to demonstrate that the phenomenon of brittle polymer hardening, as characterised by a reduction in strain

Table 7. Retention of coupon flexural stiffness post-tensile straining: aged material

Sample	Initial E_{flex}: GPa	Tensile strain to which sample was subjected: με	Subsequent E_{flex}: GPa	Original stiffness retained: %
1	18·4	6000	19·6	106
2	21·5	9000	10·0	46
3	21·3	10 000	5·8	27

Table 8. Retention of coupon flexural stiffness post-tensile straining: new material

Sample	Initial E_{flex}: GPa	Tensile strain to which sample was subjected: με	Subsequent E_{flex}: GPa	Original stiffness retained: %
1	12·5	4000	13·4	107
2	18·7	6000	20·4	109
3	18·7	6000	19·7	105
4	15·0	9000	14·7	98
5	19·4	10 000	19·3	100

limit of resin fracture, is age dependent. Flexural tests both before and after an intervening tensile loading yielded very similar results. The fact that the direct axial tensile stress did not affect flexural stiffness indicates that the resin was not affected in the coupons of the new material. Coupons of the new GFRP did not exhibit a reduction in flexural stiffness when subjected to previous axial tensile strains up to values of 10 000 με. The conclusion that a reduction in the strain limit of resin fracture is age dependent, and to a degree of such great mechanical significance, is an important finding. It confirms that design factors of safety that consider this limit must take into account the way in which this limit will change with age.

The initial flexural stiffness of some specimens (sample 1 of the aged material and samples 1 to 3 of the new material) was observed to be slightly lower than that found after straining. The stiffness of these specimens could not really increase of course, and the tolerance of the test was revealed to be as much as 10%. A variation between new and old material >10% was deemed to be significant and occurring as a consequence of the physical change in the material with ageing.

With the application of material partial safety factors, the design strength used for the design of structural elements in GFRP is typically 60% of the characteristic strength (Bank, 2006). The ultimate tensile strength of the GFRP, as defined by Strongwell, is 214 MPa. The useable design strength would therefore be around $0{\cdot}6 \times 214 = 128$ MPa. Using an elastic modulus value of 21·7 MPa (the average tensile modulus from tests presented in Figure 12), this corresponds to a maximum design strain of 5900 με. This is lower than the strain of 6000 με at which no degradation in stiffness due to polymer hardening was observed and therefore the typical material partial safety factors seem appropriate. It should be noted that in their application as building panels for the site office and Visitors, Centre (not the intended bridge enclosure application), the panel material tested will have experienced an estimated maximum strain no greater than 1000 με in service. This was verified by a structural design check accounting for both wind and occupancy actions at ultimate limit state on the structural facades.

5. Conclusions

A programme of mechanical testing of naturally aged composites taken from the Severn Bridge Visitors' Centre was undertaken to assess the durability of pultruded GFRP. In 17 years of exposure, most of the mechanical material properties do not appear to have significantly diminished below the design values, despite aesthetic quality suffering due to lack of maintenance.

Coupons of the internal material from the panels on the south- and west-facing facades outperformed those of the weathered external material in terms of tensile strength, tensile modulus and shear modulus. These elevations are those exposed to the prevailing estuary wind and rain, and those south-facing especially, to a higher degree of UV exposure. Degradation does not appear to have infiltrated the GFRP to a degree that significantly affected 'whole panel' behaviour and the design values therefore appear to be appropriate. East-, south- and west-facing panels, which experienced direct UV irradiation, all exhibited a slightly reduced stiffness when tested whole with the weathered external face in tension as opposed to the internal face in tension.

Coupon testing demonstrated that the tensile elastic modulus of the aged material, on average, met that of new material. However, the tensile strength of the aged material was lower than that of the new material. This can partly be accounted for by the observed deficit in fibre content. The comparison afforded between the new and the old is qualitative, due to fabrication and material variability remaining unknown factors despite fibre volume fractions being accounted for.

It was apparent that for all old (weathered) panel materials the tensile modulus was lower than the compressive modulus, in contrast to most reports in current research. It was hypothesised that 'polymer hardening' had occurred, leading to a brittle strain limit for the aged resin. A tensile strain of 9000 με caused severe cracking in the matrix such that the subsequent flexural stiffness was reduced by 50%. A reduction in resin plasticity with age was observed; artificial hydrothermal ageing procedures are known to maintain resin plasticity (Antoon and Koening, 1980; Liao *et al.*, 1998) and therefore appear unsuitable in the light of these findings.

Resin hardening does not completely explain the relationship between the tensile modulus and the compressive modulus because, below 6000 με (the region in which the coupon modulus was calculated), the onset of matrix cracking would probably not have been occurred. The strong influence of polymer hardening on the stiffness of the composite was very evident, and how this might improve resistance to micro-buckling of fibres in compression is the subject of further research. Further investigation of resin hardening, comparing the characteristics of aged, exposed material, with those of aged, unexposed material would also be worthy of further research.

Acknowledgements

Sincere thanks are extended to Arup and EPSRC, the sponsors of this research, without whom this work would not have been possible. Further deserved thanks are owed to Masters students Lee Westerman and Dan Culling for assisting with practical laboratory testing, Mikkel Kragh at Dow Corning for his

continuing support throughout this project, Richard Cooke at Faber Maunsell for providing the opportunity to obtain the panels, James Hennessy of Wring Group for organising the extraction and collection of the panels and Richard Irvine at Strongwell for his support in background research of the panels.

REFERENCES

Antoon MK and Koening JL (1980) The structural and moisture stability of the matrix phase in glass-reinforced epoxy composites. *Journal of Macromolecular Science – Review Macromolecular Chemistry* **19(1)**: 135–173.

ASTM (2002) D 2584-02: Standard test method for ignition loss of cured reinforced resins. ASTM International, West Conshohocken, PA, USA.

Bank LC (1989) Flexural and shear moduli of full-section fiber reinforced plastic (FRP) pultruded beams. *Journal of Testing and Evaluation* **17(1)**: 40–45.

Bank LC (2006) *Composites for Construction: Structural Design with FRP Materials*. Wiley, Hoboken, NJ, USA.

Boinard E, Pethrick RA, Dalzel-Job J and Macfarlane CJ (2000) Influence of resin chemistry on water uptake and environmental ageing in glass fibre reinforced composites-polyester and vinyl ester laminates. *Journal of Materials Science* **35(8)**: 1931–1937.

BSI (2009) Plastics – determination of tensile properties. In test conditions for unidirectional fibre-reinforced plastic composites. BSI, London, UK.

Busel JP (2002) *FRP Composites Industry Challenges in Developing New Markets*. CRC Press, Boca Raton, FL, USA.

Compston P and Dexter D (2008) The effect of ultraviolet (UV) light postcuring on resin hardness and interlaminar shear strength of a glass-fibre/vinylester composite. *Journal of Materials Science* **43(14)**: 5017–5019.

Karbhari VM, Chin JW, Hunston D *et al.* (2003) Durability gap analysis for fiber-reinforced polymer composites in civil infrastructure. *Journal of Composites for Construction* **7(3)**: 238–247.

Liao K, Schultheisz CR and Hunston DL (1998) Effects of environmental ageing on pultruded GFRP. *Composites Part B: Engineering* **30(5)**: 485–493.

OS (Ordnance Survey) (2017) http://osmaps.ordnancesurvey.co.uk/ (accessed on 29/07/2017).

Strongwell (2009) *FRP Specifications. Volume 2010*. Strongwell, Bristol, VA, USA.

Strongwell (2010) *Composolite Fibreglass Building Panel System. Volume 2010*. Strongwell, Bristol, VA, USA.

Tolf G and Clarin P (1984) Comparison between flexural and tensile modulus of fiber composites. *Fibre Science and Technology* **21(4)**: 319–326.

VPG (Vishay Precision Group) (2008) *In Plane-Shear Measurement with Strain Gauges*. Inter Technology, Toronto, ON, Canada, Technical Note 512-1.

Wang YY, Meng JY, Zhao Q and Qi SH (2010) Accelerated ageing tests for evaluations of a durability performance of glass-fiber reinforcement polyester composites. *Journal of Materials Science and Technology* **26(6)**: 572–576.

Ye BS, Svenson AL and Bank LC (1995) Mass and volume fraction properties of pultruded glass fibre reinforced composites. *Composites* **26(10)**: 725–731.